ЖУРНАЛ СТРУКТУРНОЙ ХИМИИ

2021. Том 62, № 9 *Сентябрь* *С. 1436 – 1453*

MOLECULAR STRUCTURE, FT-RAMAN, IR, NLO, NBO, HOMO—LUMO ANALYSIS, PHYSICOCHEMICAL DESCRIPTORS, ADME PARAMETERS, AND PHARMACOKINETIC BIOACTIVITY OF 2,3,5,6-TETRACHLORO-*p*-BENZOQUINONE

A. Suvitha[1], M.A.M. El-Mansy[2,3], G. Kothandan[4], A. Steephen[5]

[1]*Department of Physics, CMR Institute of Technology, Bengaluru, Karnataka, Republic of India*
E-mail: suvidanam@gmail.com
[2]*Molecular Modelling Simulation Lab., Physics Department, Faculty of Education, University of Ain Shams, Cairo, Arab Republic of Egypt*
[3]*Condensed Matter Theory Unit, College of Science and Arts, Department of Physics, Qassim University, ArRass, Kingdom of Saudi Arabia*
[4]*Biopolymer Modelling Laboratory, Centre of Advanced Study in Crystallography and Biophysics, University of Madras, Chennai, Republic of India*
[5]*Department of Physics, KPR Institute of Engineering and Technology, Tamil nadu, Republic of India*

Received	*Revised*	*Accepted*
21.12.2020	*17.04.2021*	*22.04.2021*

Vibrational, NLO, NBO, FMO, NMR substance move, and an auxiliary investigation of 2,3,5,6-tetrachloro-*p*-benzoquinone, utilizing quantum computational figuring, are performed. Atomic geometry, Mulliken charges, and vibrational wavenumbers are resolved by Hartree—Fock (HF) and DFT calculations in the B3LYP framework with the 6-311++G(*d*,*p*) premise set and confirmed by the experimental information. The potential energy distribution (PED) generates the assignments of vibrational wavenumbers. An analysis of the electronic properties is carried out using the time-autonomous DFT technique, providing HOMO and LUMO energies. Molecular electrostatic potential (MEP), natural bond orbitals (NBO), and nonlinear optical (NLO) properties are also reported. ^{13}C and ^{1}H NMR synthetic movements are distinguished by the GIAO procedure and diverged from the test substance move. The TED commitment as a blended mode with different vibrations is around 75 %. Physicochemical descriptors, ADME boundaries, pharmacokinetics, pH significance, medicative and restorative nature are processed for the title compound. These properties are computed utilizing a computer aided drug design to encourage the sedate disclosure.

DOI: 10.26902/JSC_id79909

K e y w o r d s: 2,3,5,6-tetrachloro-*p*-benzoquinone (TCBQ), NBO, NLO, HOMO—LUMO, ADME, MEP, CADD.

INTRODUCTION

Quinone contains two carbonyl groups and belongs to the class of cyclic organic compounds that play a significant role in different controls going from biophysics to natural science [1]. 2,3,5,6-Tetrachloro-*p*-benzoquinone (TCBQ) is a quinone derivative with the molecular formula $C_6C_{l4}O_2$, and it is in the form of a yellow solid. *p*-Quinone is applied essentially as a forerunner to hydroquinone utilized in photography and as an elastic producer [2]. It is a planar atom capable of being a gentle oxidant and filling in as a hydrogen acceptor [3]. This is primarily used for aromatization reactions,

such as converting cyclohexadienes to benzene derivatives [4]. It is utilized as a fungicide and seed defender with optional creepy crawly repellent and bactericidal impacts in its immediate discharge to nature. It is used as a dye intermediate, in the manufacture of electrodes for pH measurements or a reagent that may result in its release into various waste streams through the environment [5]. It is also applied as seed treatment for a variety of field and vegetable crops [6]. Bianchini et al. [7] performed a study on the molecular orbital calculations of unsubstituted quinone using Co-quinoid complexes. Gordon et al. [8] have given an account of the incorporation of the free quinone ligand in an investigation of the holding of metal-quinone edifices. The study by Daniel E. Wheeler et al. [9] reported the DFT study of electronic structure varieties over the *ortho* quinone/semi quinone/catechol redox series. At a subatomic orbital level, Al-Sabha et al. [10] investigated the use of chloranil and fluoranil in the spectrophotometric assurance of mesalamine in pharmaceuticals to treat π-acceptors. As nutrients, they correspond to a class of atoms that forestall and treat a few illnesses, for example, osteoporosis and cardiovascular ailments. Quinones, by their cancer prevention agent action, improve general wellbeing conditions. A significant number of medications are clinically endorsed or still in clinical preliminaries against quinone-related mixes [11]. Chihara H. et al. [12] have reported FTIR, UV spectra of TCBO in the NIST Standard Reference Data Program. In this manner, broad examinations have been completed on the quinone subordinates to depict attractive properties. Overall, this compound has applications in chemical laboratories, pharmaceuticals, polymers, intermediates, agricultural processing, forestry, and fishing. Furthermore, TCBQ is used to make rubber, plastic and electrical, electronic, and optical devices, among other things.

The literature survey reveals that neither quantum computational (DFT) nor computer-aided drug designing approaches have been undertaken so far on TCBO. Thus, the present study is carried out on TCBQ in order to carry out the complete vibrational and structural analysis and also to study the electronic charge transitions, MEP, NBO, NLO, HOMO and LUMO, chemical shifts, and stabilization energy were calculated by Gaussian techniques and ADME boundaries, pharmacokinetics, pharmacodynamics, nature and bioactivity by web programming tools.

EXPERIMENTAL

A blend of IR spectra in the KBr pellet technique for IR 2 cm^{-1} sweeps and 100 quantities of MIR 4000—400 cm^{-1} with a FTIR spectrometer scope were obtained using PerkinElmer Spectrum. A BRUKER optics RFS 27 FT-Raman spectrometer was used in the range 4000—50 cm^{-1} for recording FT-Raman spectra. ^{13}C NMR was taken from the National Medicine Library database, PubChem. Spectral data are from the NIST Chemistry Webbook-UV.

Computational details. DFT computations were carried out using the Gaussian09 [13] and Gauss view [14] applications with a high-end machine without any restrictions. The B3LYP-6-311++G(*d,p*) command is most important to calculate the runtime program and to interpret the Gaussian output data. Vibrational modes were determined by the vibrational energy distribution analysis (VEDA 4) with vibrational assignments dependent on the potential vitality appropriation (PED) strategy [15]. The Gaussian package also includes the molecular structure optimization, the HOMO—LUMO vitality gap, the subatomic electrostatic potential, and electronic excitation of DMSO and gas in various dissolvable states. The same basis set was used to analyze the ligands by NBO [16], NLO, Mulliken charges, and ^{1}H and ^{13}C NMR. Origin and Gab edit, and Adobe Photoshop software were also used to interpret the graphical diagrams and tables. Marvin sketch was used to find descriptors, chemical compositions, and log P values in anionic and non-ionic species, pH micro-species distribution, topology and confirmed the molecular structure [17]. ADME parameters, pharmacophore modeling, drug-like nature, pharmacokinetics/pharmacodynamics, metabolism, biological activity radar are calculated by the Swiss ADME software [18].

RESULTS AND DISCUSSION

Structural analysis

Fig. 1 illustrates the particle chemical structure, optimum geometry, and Van der Waals spheres with atomic numbering. TCBQ is a non-straight, 12-particle compound. Therefore, under the C_1 group symmetry, there are $(3 \cdot 12 - 6 = 30)$ disseminated ordinary vibrational modes.

$$\Gamma \text{ vib} = 21A' + 9A''.$$

All these vibrational modes are seen in the reported FTIR and FT-Raman spectra. A′ stands for in-plane vibrations and A″ mean out-of-plane vibrations. Table 1 presents the definite PED tasks and hypothetical wavenumbers with hypothetical scaled and unscaled frequencies, force constants, IR speed, and Raman operations. Fig. 2*a*, *b* displays separately the recorded and computed (6-311++G(*d*,*p*) in HF and B3LYP) FTIR and FT-Raman spectra of present particles.

IR and FT-Raman Vibrational Analyses

Ring vibrations. The ring extending vibrations of quinone and its subordinates have the idealistic character of the aromatic ring. The majority of the aromatic mixes are around 1620—1390 cm^{-1}

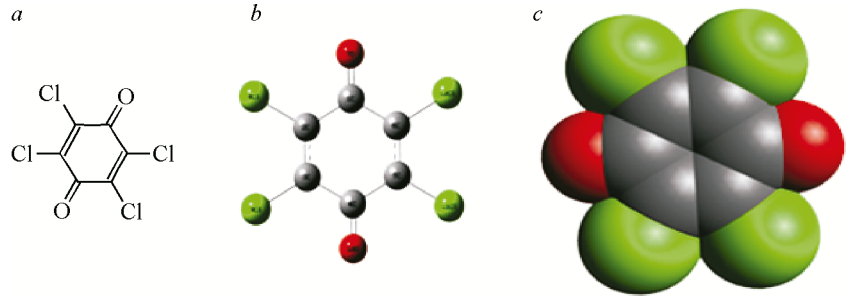

Fig. 1. Chemical (*a*) and optimum geometry (*b*), Van der Waals spheres (*c*) for TCBQ

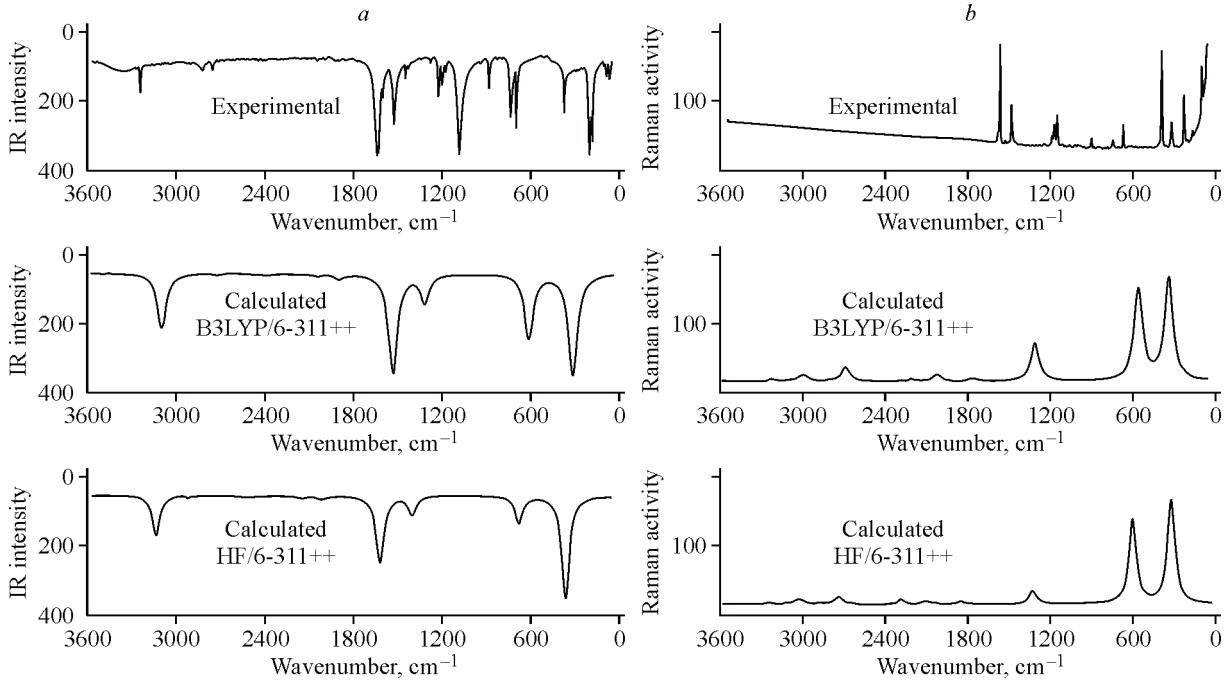

Fig. 2. Experimental and simulated FTIR (*a*) and FT-Raman (*b*) spectra for TCBQ

Table 1

Recorded and theoretical FTIR, FT-Raman *wavenumbers*, IR *intensities and corresponding assignments for* TCBQ

Sr. N	Experimental F, cm^{-1}		Computed F, cm^{-1}		Computed F, cm^{-1}		Computed values			C_1	Assignments with PED (≥10 %)
	FTIR	FT-Raman	HF-6-311++		B3LYP-6-311++		B3LYP-6-311++				
			Unscaled	Scaled	Unscaled	Scaled	K	I^{IR}	S^a		
1	2	3	4	5	6	7	8	9	10	11	12
1	1700s		2005	1818	1754	1724	24.04	413.52	0.00	A′	ν(O7—C1)(47), ν(O10—C4)(47)
2		1690s	1997	1811	1753	1723	24.07	0.00	202.21	A′	ν(O7—C1)(48), ν(O10—C4)(48)
3	1680s		1834	1663	1634	1606	18.89	0.00	180.69	A′	ν(C2—C3)(35), ν(C5—C6)(45)
4	1650m		1802	1634	1595	1567	18.01	258.16	0.00	A′	ν(C2—C3)(44), ν(C5—C6)(44)
5	1260m	1260w	1388	1258	1229	1208	10.71	0.00	73.18	A′	ν(C1—C2)(23), ν(C3—C4)(27), β(C4—C5—C6)(18)
6		1240m	1355	1229	1217	1196	10.57	110.84	0.00	A′	ν(C1—C2)(28), ν(C4—C5)(12)
7	1210vw		1220	1106	1101	1083	8.71	401.49	0.00	A′	β(C4—C5—C6)(29), β(C2—C3—C4)(21), β(C3—C4—C5)(12)
8	1110vs		1070	970	986	969	7.39	0.00	4.75	A′	ν(C3—C4)(22), ν(C4—C5)(16), ν(Cl8—C2)(10), ν(Cl9—C3)(10), ν(Cl11—C5)(10), ν(Cl12—C6)(10)
9		1000w	975	884	906	890	6.26	17.41	0.00	A′	β(C1—C2—C3)(10), β(C3—C4—C5)(28)
10	900w		916	831	845	830	5.68	0.00	12.54	A′	ν(C3—C4)(11), ν(Cl8—C2)(15), ν(Cl9—C3)(15), ν(Cl11—C5)(15), ν(Cl12—C6)(15)
11		850vw	803	728	748	735	4.01	0.00	2.51	A′	τ(C1—C6—C5—C4)(11), λ(O10—C3—C5—C4)(39), λ(O7—C2—C6—C1)(39)
12		770w	802	727	737	724	3.91	12.85	0.00	A′	λ(O10—C3—C5—C4)(39), λ(O7—C2—C6—C1)(39)
13	750s		797	723	733	721	4.71	204.66	0.00	A′	ν(Cl8—C2)(18), ν(Cl9—C3)(18), ν(Cl11—C5)(18), ν(Cl12—C6)(18), β(C2—C1—O7)(11), β(C5—C4—O10)(11)

Continued Table 1

1	2	3	4	5	6	7	8	9	10	11	12
14	710s		789	715	730	717	3.98	0.00	0.10	A′	β(C2—C1—O7)(29), β(C5—C4—O10)(29), β(C3—C2—CL8)(10)
15		500vs	617	559	547	538	2.15	0.00	0.00	A″	τ(C1—C6—C5—C4)(18), τ(Cl11—C5—C6—Cl12)(32), λ(Cl9—C2—C4—C3)(21), λ(Cl8—C1—C3—C2)(21)
16		490w	525	476	488	480	2.07	0.00	27.43	A″	ν(C2—C3)(15), ν(C3—C4)(10), β(C1—C2—C3)(17), β(C2—C3—C4)(12), β(C3—C4—C5)(10)
17	480vw		503	456	466	458	2.77	4.95	0.00	A′	ν(Cl8—C2)(16), ν(Cl9—C3)(16), ν(Cl11—C5)(16), ν(Cl12—C6)(16), β(C4—C5—C6)(12), β(C1—C2—C3)(13)
18		430w	448	406	415	408	1.27	0.00	0.71	A′	τ(C1—C2—C3—C4)(10), τ(Cl11—C5—C6—Cl12)(36), λ(Cl9—C2—C4—C3)(19), λ(Cl8—C1—C3—C2)(19)
19	380m		416	377	380	374	1.52	4.62	0.00	A′	β(C2—C1O7)(29), β(C5—C4—O10)(29)
20		340m	369	335	338	333	1.24	0.00	2.32	A′	ν(C3—C4)(11), β(C2—C1—O7)(11), β(C5—C4—O10)(11), β(C3—C2—Cl8)(11)
21		330vw	346	314	322	317	1.66	0.00	8.77	A″	ν(C3—C4)(13), ν(C4—C5)(13), β(C3—C4—C5)(28)
22		300vw	335	304	302	297	0.68	0.00	3.14	A″	λ(Cl11—C4—C6—C5)(51), λ(Cl9—C2—C4—C3)(24), λ(Cl8—C1—C3—C2)(24)
23		260w	289	262	264	260	0.99	0.00	0.32	A″	β(C4—C5—C6)(14), β(C1—C2—C3)(12)
24	200vs	200vs	233	211	214	210	0.86	0.16	0.00	A″	β(C3—C2—Cl8)(22), β(C4—C3—Cl9)(21), β(C4—C5—Cl11)(21), β(C1—C6—Cl12)(21)
25		190vw	217	197	203	200	0.61	0.04	0.00	A′	β(C3—C2—Cl8)(15), β(C4—C3—Cl9)(19), β(C4—C5—Cl11)(19), β(C1—C6—Cl12)(19)
26	180vs		216	196	199	196	0.81	0.00	3.46	A′	β(C3—C2—Cl8)(26), β(C4—C3—Cl9)(22), β(C4—C5—Cl11)(22), β(C1—C6—Cl12)(22)

Continued Table 1

1	2	3	4	5	6	7	8	9	10	11	12
27	150w		202	183	180	177	0.26	4.76	0.00	A′	λ(O10—C3—C5—C4)(11), λ(O7—C2—C6—C1)(11), λ(Cl11—C4—C6—C5)(39), λ(Cl9—C2—C4—C3)(18), λ(Cl8—C1—C3—C2)(18)
28	80w		78	71	79	77	0.07	0.00	0.04	A″	τ(C1—C6—C5—C4)(34), τ(C1—C2—C3—C4)(38), τ(Cl11—C5—C6—Cl12)(10)
29		70w	68	62	61	60	0.07	0.00	0.00	A″	τ(C1—C6—C5—C4)(32), τ(C1—C2—C3—C4)(41), τ(Cl11—C5—C6—Cl12)(19)
30	50w		41	37	48	47	0.03	2.09	0.00	A″	τ(C2—C3—C4—C5)(92)

Abbreviations: vs — very strong; s — strong; m — medium; w — weak; F — frequency; z[ν = stretching, β = bending, τ = torsion, λ = out of plane]; K — force constant; I^{IR} — Intensity of IR; S^a — activity in Raman; C_1 — point group symmetry.

because of ring CC extending groups [19—21]. As anticipated in the prior references, the TCBQ particle offers ascend to two C=C extending groups found at 1606 cm^{-1} and 1567 cm^{-1} with strong and medium forces. The figured features of C=C extending vibrations actually correspond to the observed features. The vibrational groups are located separately at 1208 cm^{-1}, 1196 cm^{-1}, 969 cm^{-1}, and 830 cm^{-1} due to C—C expanding vibrations occurring in the ring. These tasks do not agree with the other reported estimates; thus, it might be concluded that these modes are marginally impacted by different modes. The features of these groups demonstrate that the skeletal modes are somewhat higher than their standard values. It suggests that the carbonyl gathering supported these skeletal vibrations. Sarojini and coworkers note that C—C—C wavenumber is within the range of 999—665 cm^{-1} [22]. For TCBQ, at the B3LYP-6-311++G(*d*,*p*) level, the C—C—C planar ring vibrations are predicted to be at 1038 cm^{-1}, 830 cm^{-1}, 480 cm^{-1}, and 458 cm^{-1}, but these vibrations are tentatively observed in the IR spectra at 1210 cm^{-1}, 900 cm^{-1}, and 480 cm^{-1}. C—C—C—C non-planar vibrations of TCBQ are compared with the determined wavenumbers of 735 cm^{-1} and 538 cm^{-1}. These vibrations are at 850 cm^{-1} and 500 cm^{-1} in the Raman spectra. They were interpreted as torsion deformation modes (CCCC) and listed in Table 1.

C=O vibrations. In TCBQ, the benzene ring is associated with two C=O groups and thus, gives up to two C=O extensions; two C=O in-plane and two C=O out-of-plane twisting vibrations. The C=O extension is usually seen in the range of 1700—1800 cm^{-1} [23]. In the current examination, the recorded IR-Raman bands are observed at 1690 cm^{-1} and 1700 cm^{-1}, which could be designated as C=O extending vibrations. The DFT/B3LYP has 94 % and 96 % TED dedication, showing mild rivalry with knowledge on testing and writing. The related C=O in-plane and out-of-plane twisting is estimated at 717 cm^{-1}, 374 cm^{-1} and 735 cm^{-1}, 724 cm^{-1}, respectively. Such whole C=O modes are quite well within a nearly equal range reported previously [24]. Subsequently, it might be reasoned that the carbonyl vibrations are very little influenced by other vibrionic groups.

C—Cl vibrations. The carbonyl dynamics has a position with bonds of C (X = F, Cl, Br) positioned between the benzene ring and the halogen molecules. The most part of the C—Cl extending vibrations fall in the range of 800—700 cm^{-1} [25—27]. The C—Cl extending vibrations are observed at 969 cm^{-1}, 830 cm^{-1}, 721 cm^{-1}, and 458 cm^{-1}; they somewhat deviate from the anticipated area because of the impact of useful gathering. The hypothetically processed features show good agreement with the experimental information. Two reasons might be responsible for the higher move of C—Cl in TCBQ. The former is caused by vibrational holding with different particles, and the latter is a persuasive inductive form of the C—Cl bond. Considering that the chlorine atom has a higher electronegativity than the carbon ion, the holding electrons in the C—Cl bond would be closer to the chlorine ion

Table 2

Study of Fock matrix perturbation theory in the NBO *basis for* TCBQ

I	Type of band	Occu-pancy	*J*	Type of band	Occu-pancy	*E*2, kJ/mol[#1]	*E*(*j*)—*E*(*i*), a.u.[#2]	*F*(*i*,*j*), a.u.[#3]
1	2	3	4	5	6	7	8	9
C1—C2	σ	1.973	C1—C6	σ*	0.083	0.52	1.02	0.021
		1.973	C1—O7	σ*	0.007	0.6	1.18	0.024
		1.973	C2—C3	σ*	0.038	2.37	1.2	0.048
		1.973	C3—Cl9	σ*	0.026	5.12	0.8	0.057
		1.973	C6—Cl12	σ*	0.026	2.59	0.8	0.041
C1—C6	σ	1.973	C1—C2	σ*	0.083	0.52	1.02	0.021
		1.973	C1—O7	σ*	0.007	0.6	1.18	0.024
		1.973	C2—Cl8	σ*	0.026	2.59	0.8	0.041
		1.973	C5—C6	σ*	0.038	2.37	1.2	0.048
		1.973	C5—Cl11	σ*	0.026	5.12	0.8	0.057
C1—O7	σ	1.994	C1—C2	σ*	0.083	1.09	1.36	0.035
		1.994	C1—C6	σ*	0.083	1.09	1.36	0.035
		1.994	C2—C3	σ*	0.038	0.9	1.54	0.033
		1.994	C5—C6	σ*	0.038	0.9	1.54	0.033
C1—O7	π	**1.941**	**C2—C3**	π*	**0.239**	**6.18**	**0.35**	**0.044**
		1.941	**C5—C6**	π*	**0.239**	**6.18**	**0.35**	**0.044**
C2—C3	σ	1.989	C1—C2	σ*	0.083	1.4	1.11	0.036
		1.989	C1—O7	σ*	0.007	1.04	1.28	0.033
		1.989	C3—C4	σ*	0.083	1.4	1.11	0.036
		1.989	C4—O10	σ*	0.007	1.04	1.28	0.033
C2—C3	π	**1.854**	**C1—O7**	π*	**0.166**	**14.33**	**0.3**	**0.059**
		1.854	**C4—O10**	π*	**0.166**	**14.33**	**0.3**	**0.059**
C2—Cl8	σ	1.986	C1—C6	σ*	0.083	1.74	1.06	0.039
		1.986	C2—C3	σ*	0.038	0.61	1.24	0.025
		1.986	C3—C4	σ*	0.083	3.25	1.06	0.053
C3—C4	σ	1.973	C2—C3	σ*	0.038	2.37	1.2	0.048
		1.973	C2—Cl8	σ*	0.026	5.12	0.8	0.057
		1.973	C4—C5	σ*	0.083	0.52	1.02	0.021
		1.973	C4—O10	σ*	0.007	0.6	1.18	0.024
		1.973	C5—Cl11	σ*	0.026	2.59	0.8	0.041
C3—Cl9	σ	1.986	C1—C2	σ*	0.083	3.25	1.06	0.053
		1.986	C2—C3	σ*	0.038	0.61	1.24	0.025
		1.986	C4—C5	σ*	0.083	1.74	1.06	0.039
C4—C5	σ	1.973	C3—C4	σ*	0.083	0.52	1.02	0.021
		1.973	C3—Cl9	σ*	0.026	2.59	0.8	0.041
		1.973	C4—O10	σ*	0.007	0.6	1.18	0.024
		1.973	C5—C6	σ*	0.038	2.37	1.2	0.048
		1.973	C6—Cl12	σ*	0.026	5.12	0.8	0.057
C4—O10	σ	1.994	C2—C3	σ*	0.038	0.9	1.54	0.033
		1.994	C3—C4	σ*	0.083	1.09	1.36	0.035
		1.994	C4—C5	σ*	0.083	1.09	1.36	0.035

Continued Table 2

1	2	3	4	5	6	7	8	9
		1.994	C5—C6	σ*	0.038	0.9	1.54	0.033
C4—O10	π	**1.941**	**C2—C3**	π*	**0.239**	**6.18**	**0.35**	**0.044**
		1.941	**C5—C6**	π*	**0.239**	**6.18**	**0.35**	**0.044**
C5—C6	σ	1.989	C1—C6	σ*	0.083	1.4	1.11	0.036
		1.989	C1—O7	σ*	0.007	1.04	1.28	0.033
		1.989	C4—C5	σ*	0.083	1.4	1.11	0.036
		1.989	C4—O10	σ*	0.007	1.04	1.28	0.033
C5—C6	π	**1.854**	**C1—O7**	π*	**0.166**	**14.33**	**0.3**	**0.059**
		1.854	**C4—O10**	π*	**0.166**	**14.33**	**0.3**	**0.059**
C5—Cl11	σ	1.986	C1—C6	σ*	0.083	3.25	1.06	0.053
		1.986	C3—C4	σ*	0.083	1.74	1.06	0.039
		1.986	C5—C6	σ*	0.038	0.61	1.24	0.025
C6—Cl12	σ	1.986	C1—C2	σ*	0.083	1.74	1.06	0.039
		1.986	C4—C5	σ*	0.083	3.25	1.06	0.053
		1.986	C5—C6	σ*	0.038	0.61	1.24	0.025

Donor: *I*; receiver: *J*

[#1] *E*2 means hyper conjugative energy interactions.

[#2] Differential energy between *i* and *j*. Orbitals to NBO.

[#3] $F(i, j)$ is an element of the Fock matrix between *i* and *j*. Orbitals at NBO.

than to the carbon ion, increasing stable power and providing a lower recurrence period. The 717 cm^{-1} band corresponds to C—Cl in-plane twisting vibrations. The processed estimates for CCl in-plane twisting dynamics are in agreement with the IR calculated values for TCBQ [28]. This indicates that the C—Cl movements lie entirely in an alternative field and are not affected by specific modes.

NBO analysis. The current particle analysis is performed using the of DFT-B3LYP approach with a 6-311++ basis set and the results are gathered in Table 2. The single benzene ring has clearly shown a strong delocalization of electrons within the ring. An increase in the *E*2 vitality for various advances between these donors and acceptors suggests that the chances of the following advances are highly likely: C4—O10 to C2—C3/C5—C6 (6.18 kJ/mol, π*), C2—C3 to C1—O7/C4—O10 (14.33 kJ/mol, π*), and C5—C6 to C1—O7/C4—O10 (14.33 kJ/mol, π*). The quantity of hydrogen bond acceptors is 2 and the number of benefactors of H bonds is 0, which is confirmed in Table 9. The examination of these plausible changes uncovers that just one progress is exceptionally likely (C2—C3/C5—C6 → → C1—O7/C4—O10) and the other are just the duplication of these advances, which confirms that the π → π* transitions are highly probable.

Frontier molecular orbitals (FMOs). The HOMO and LUMO of the title compound are calculated at the same B3LYP/6-311++G(*d*,*p*) level and depicted in Fig. 3. HOMO, HOMO–1, LUMO, and LUMO+1 of TCBQ were calculated at the B3LYP/6-311++G(*d*,*p*) level in gas and solvents (DMSO and chloroform) to test the thermochemical properties. The HOMO and LUMO gap is larger in the gas state as compared with that in the two solvents (3.27 eV). Significant changes are figured with the Gauss sum program [29] and the features are introduced in Table 3.

UV-Vis spectral analysis. Fig. 4 shows the B3LYP6-311++ theoretical (*a*), DOS charts (*b*), and experimental (*c*) results for TCBQ in the gas phase. UV spectral data were borrowed from the NIST Chemistry Webbook [30]. The oscillator quality (*f*) values for the six plausible advances are recorded and it is discovered that the f value is about zero for five advances, and one $f = 0.1611$ a.u., which might be C2—C3/C5—C6 →C1—O7/C4—O10, as the adjustment vitality is high for this progress.

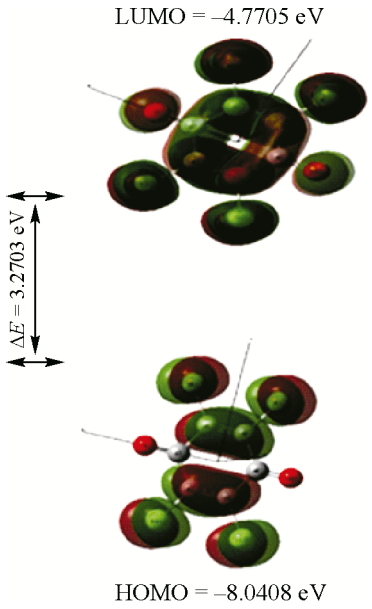

Fig. 3. HOMO and LUMO orbitals of the TCBQ gas phase

T a b l e 3

TCBQ *energy values in the gas state and solvents* (DMSO *and chloroform*) *calculated for thermochemistry*

TD-SCF/B3LYP/6-311++G(*d*,*p*)	Gas	DMSO	Chloroform
E_{total}, Hartree	–2220.003	–2220.013	–2220.009
E_{HOMO}, eV	8.0408	7.8316	7.8942
E_{LUMO}, eV	4.7705	4.6290	4.6758
$\Delta E_{HOMO—LUMO\ gap}$, eV	3.2703	3.2026	3.2184
$\Delta E_{HOMO—LUMO\ gap}$ (eV)	3.2703	3.2026	3.2184
$E_{HOMO–1}$, eV	8.5396	8.3834	8.4316
E_{LUMO+1}, eV	2.2776	2.0436	2.1171
$\Delta E_{HOMO–1—LUMO+1\ gap}$, eV	6.6262	6.3398	6.3145
Electronegativity (χ), eV	6.4056	6.2303	6.285
Chemical hardness (η), eV	1.6351	1.6013	1.6092
Softness (ζ), eV^{-1}	0.61158	0.62449	0.62142
Electrophilicity index (ψ)	12.547	12.1203	12.273

The assimilation frequency for this change is 346.26 nm in the gas state. To confirm this expectation, the figured UV-Vis retention range shows a single band at 346 nm; 92 % of the contribution shown in Table 4.

Mulliken atomic charge analysis. The Mulliken charges are the charges situated in the neighborhood electron density (charge density). It unequivocally depends on the fundamental set and is useful in light of the fact that it is sensitive to the likelihood density. The atomic polar tensor (APT) and Mulliken population research uses a collection of DFT techniques to measure nuclear charges on the atoms and explains the features gathered in Table 5. Graphical representations of the nuclear charges are shown in Fig. 5. Table 5 shows (on account of both Mulliken and APT at the B3LYP/6-311++G(*d*,*p*) level) that among the carbon molecules, two C_1 and C_4 carbon atoms have more negative charges (–1.839C and –1.839C) than other carbon atoms because of the replacement of ketone moieties,

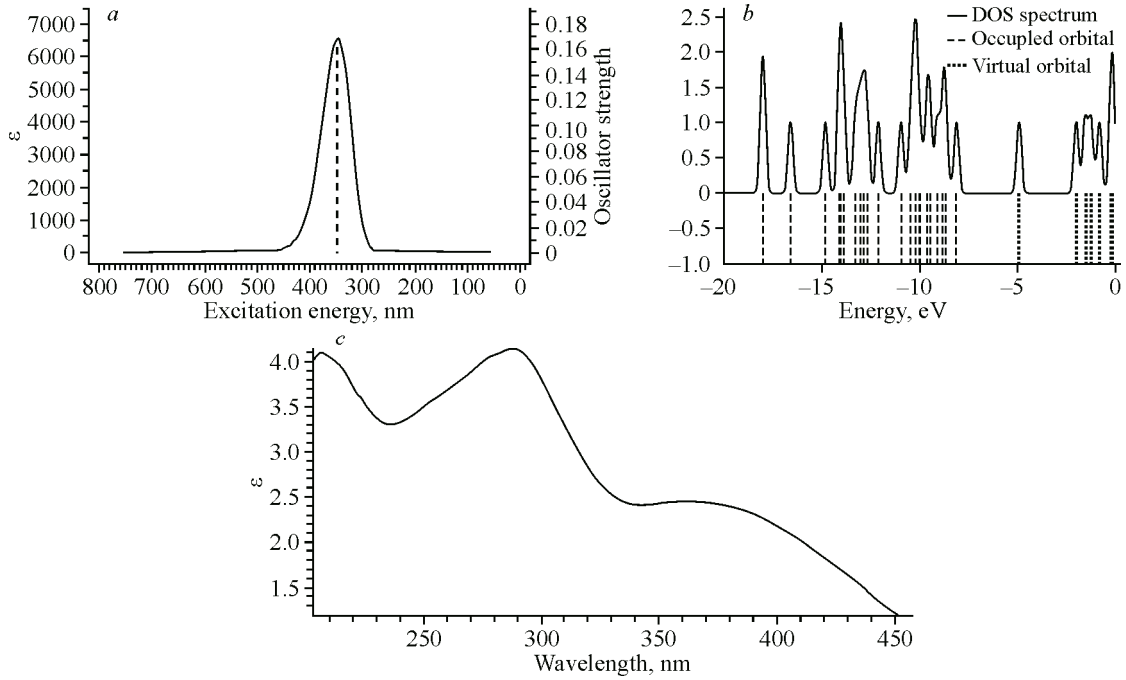

Fig. 4. UV spectrum: B3LYP6-311++ theoretical (*a*), DOS charts (*b*), and experimental (*c*) for TCBQ in the gas phase

T a b l e 4

Calculated absorption wavelength λ, *E and f of* TCBQ *at the* B3LYP-6-311++G(*d*,*p*) *level*

Parameter	λ, nm	*E*, eV	*f*, a.u.	Major contribution
Gas	488.12	2.5401	0.0	H → L (100 %)
	460.85	2.6903	0.0	H—2 → L (97 %)
	457.39	2.7107	0.0	H—3 → L (98 %)
	346.26	**3.5807**	**0.1611**	H—1 → L (92 %)
	332.64	3.7273	0.0	H—4 → L (98 %)
	321.02	3.8621	0.0	H—5 → L (99 %)
DMSO	506.32	2.4484	0.0	H → L (100 %)
	441.85	2.8060	0.0	H—2 → L (96 %)
	437.31	2.8352	0.0	H—3 → L (98 %)
	355.15	3.4910	0.2297	H—1 → L (94 %)
	330.69	3.7493	0.0	H—4 → L (97 %)
	319.11	3.8853	0.0001	H—5 → L (99 %)
Chloroform	502.33	2.4682	0.0	H → L (100 %)
	448.36	2.7653	0.0	H—2 → L (96 %)
	444.11	2.7917	0.0	H—3 → L (98 %)
	354.97	3.4929	0.2325	H—1 → L (94 %)
	332.26	3.7315	0.0	H—4 → L (97 %)
	320.64	3.8667	0.0001	H—5 → L (99 %)

N o t e. HOMO — H; LUMO — L; *f* — oscillator strength.

T a b l e 5

Mulliken and APT *atomic charges of* TCBQ

Atoms	B3LYP/6-311++	
	Mulliken charges, c	APT atomic charges, C
1 C	–1.839703	–1.964661
2 C	0.488268	0.668514
3 C	0.488268	0.668514
4 C	–1.839703	–1.964661
5 C	0.488268	0.668514
6 C	0.488268	0.668514
7 O	–0.121047	0.17125
8 Cl	0.492107	0.228191
9 Cl	0.492107	0.228191
10 O	–0.121047	0.17125
11 Cl	0.492107	0.228191
12 Cl	0.492107	0.228191

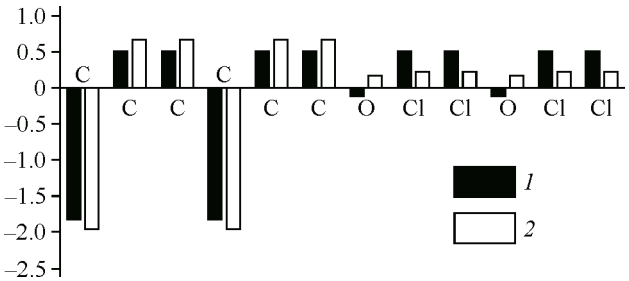

Fig. 5. Graphical depictions of Mulliken (*1*) and APT (*2*) atomic charges on TCBQ

cipated to be somewhat negative, which may be due to conjugation of electrons from the neighboring atoms. All the Cl atoms are seen as positive with Mulliken and APT 0.492C and 0.228C values at the B3LYP level.

NMR spectrum and calculations. ^{13}C chemical shift computations of the compound were based on a gauge-independent atomic orbital (GIAO) method combined with the B3LYP strategy. The hypothetical estimates of ^{13}C NMR shifts along with the experimental information gathered [31, 32] are introduced in Table 6; the pictorial representation is shown in Fig. 6.The carbon shifts in the benzene ring range from 120 ppm to 160 ppm by and large. Due to the ketone and chlorine substitution, the calculated shifts are higher than normal. Since the C1 and C4 carbon atoms are connected with the ketone group, the most extreme shifts are found for both C1 and C4 with a value of 182.47 ppm, which are seen as more adversely charged in the Mullikan examination. This is due to the oxygen conjugation or a high electronegative property of the oxygen atom. The other carbon atoms have slightly lower shifts around 159 ppm.

MEP. The 3D simulated subatomic electrostatic potential (MEP) plot with the TCBQ contour map appears in Fig. 7. It depends on the electron density at different points. MEP has the order red < orange < yellow < green < blue (see the electronic version). The shading codes of the title compound are in the range from –4.450 e^{-2} (the deepest red) to +4.450 e^{-2} (the deepest blue). As shown in Fig. 7, oxygen molecules exhibit an –ive potential and chlorine atoms have a +ive potential in the range concerned. Same expectation is referenced in translation on Mulliken nuclear charges. The subsequent surface all the while shows a subatomic size and shape and a possible electrostatic value.

Table 6

Calculated and measured ^{13}C NMR *isotropic chemical shifts* (ppm) *of* TCBQ

Atoms	B3LYP/6-311++ computed	Expt. (Ref [32])
C1	182.466	169.4
C4	182.466	169.4
C2	159.13	139.4
C3	159.13	139.4
C5	159.13	139.4
C6	159.13	139.4

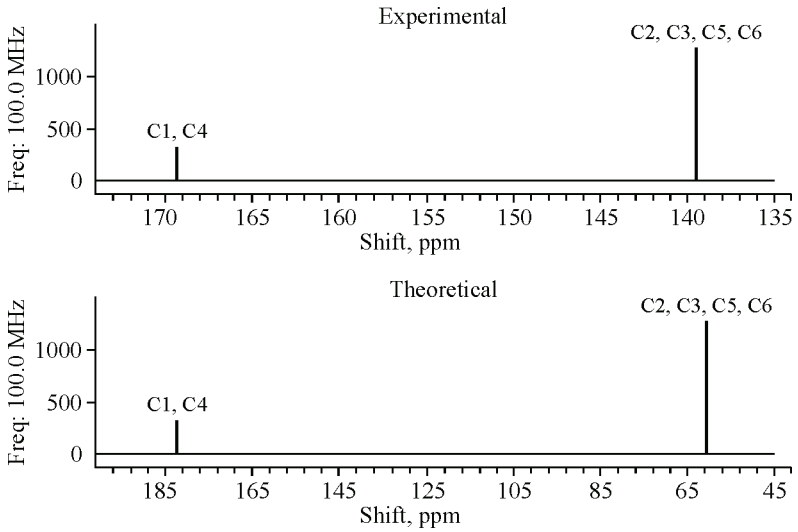

Fig. 6. Computed and theoretical ^{13}C NMR spectra of TCBQ

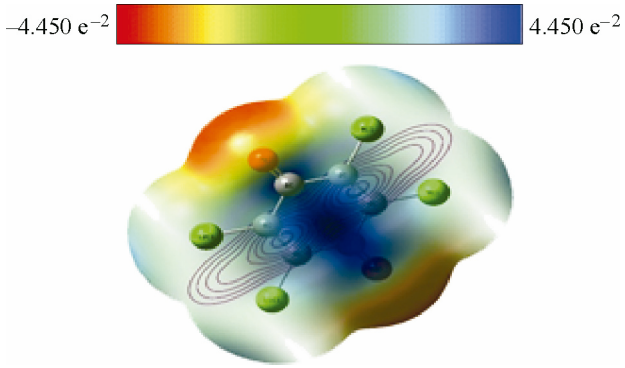

Fig. 7. MEP of TCBQ

NLO effect. The NLO effect arises from electromagnetic field interactions in different media to create new fields different in point, recurrence, adequacy or other attributes resulting from episode fields. The enormous nonlinearities shown by π-conjugated particles and polymers coupled with their ultrafast reaction are ideal for the identification of these applications. Second-request NLO materials, for example, are promising for their application in fast electro-optical modulators and switches, while third-request mixtures are promising for all optical exchanging, registering, and constraining gadgets [33]. The molar refractivity of TCBQ is 47.48. The hyperpolarizability of the first order β, the hyper-

Table 7

TCBQ *electric dipole moment*, *polarization*, *first and second order hyperpolarizability*

Polarizability (α)	a.u.	e.su ($\times 10^{-24}$)	Hyperpolarizability in first order (β)	a.u.		Hyperpolarization of second order (γ)	e.su ($\times 10^{-33}$)
α_{xx}	139.0	20.601	β_{xxx}	0	0	γ_{xxx}	6.304
α_{xy}		0	β_{yxx}	0	0	γ_{yxx}	–10.17
α_{yy}	175.2	25.967	β_{xyy}	0	0	γ_{xyy}	3.869
α_{xz}	0	0	β_{yyy}	0	0	γ_{yyy}	0
α_{yz}	0	0	β_{zxx}	0	0	γ_{zxx}	0
α_{zz}	61.87	9.170	β_{xyz}	0	0	γ_{xyz}	0
α_{tot}	125.3	18.580	β_{zyy}	0	0	γ_{zyy}	—
$\Delta\alpha$	100.3	14.861	β_{xzz}	0	0	γ_{xzz}	—

polarizability of the second order γ, the second dipole moment μ, and the polarizability α were determined using B3LYP-6-311++G(*d*,*p*) based on the limited field approach. Table 7 presents the recorded complete static second dipole moment μ, the mean polarizability α_{tot}, the polarizability anisotropy α, and the mean first hyperpolarizability β for the examined atoms.

The table shows that the polarizability anisotropy of the compound is 14.861 ($\times 10^{-24}$ e.su), the mean polarizability is 18.58 ($\times 10^{-24}$ e.su), the main hyperpolarizability is zero, and the all-out second dipole moment is also zero. Therefore, there is no much reaction of the principal request hyperpolarizability. Furthermore, the second-request hyperpolarizability was examined similarly. The γ values (a.u.) are 6.304, –10.17, 3.86, which assumes a significant NLO effect. Generally, it is utilized in fast electro-optical modulators and switches, which affirms that the compound gives more applications in photography and elastic assembling as a diminishing specialist and cancer prevention agent.

Structural analysis. Table 8 documents TCBQ structural boundaries calculated by HF and B3LYP with the 6-311++G(*d*,*p*) basis set. The calculated bond lengths and bond angles were compared with the corresponding experimental data [34]. The comparison diagram is shown in Fig. 8 for the TCBQ bond lengths and bond angles. From the table it is very well seen that the C—Cl bond length is ~1.72 Å in both HF and B3LYP results. This is somewhat different from the experimental value of 1.76 Å, which shows that the C—Cl bond length is less affected by the other substitutions, and this has been properly recognized in theoretical techniques. All C—C bond lengths in the benzene ring are similar (1.5 Å) and vary widely with the C=C bond lengths (1.3 Å); here the bond lengths are similar to the experimental value and this states that both single and double C—C bond lengths are not affected by substituents. Since there is no rotatable bond in this molecule, which is also confirmed in Table 9, both C—O bond lengths contained are 1.18 Å in HF and 1.21 Å in B3LYP. This indicates that the B3LYP technique was very much in line with the experimental value.

Many of the bond angles within the benzene ring (CCC) and outside the ring (CCO) are 121.5° in B3LYP, which indicates that the hexagonal benzene ring is distorted due to the replacement of Cl and oxygen atoms. Yet, the other bond angles inside the ring (C2—C1—C6 and C3—C4—C5) are 117°. As for C—C—Cl, these bond angles are ~115° and 123°.

Biological activity and ADME properties. Swiss ADME was utilized to process the physicochemical descriptors just as to foresee ADME boundaries, pharmacokinetic properties, tranquilization nature, and therapeutic activity of TCBQ (Table 9). It can be imagined that the organic action of this compound might be emerging from the quinone ring, which may assume a significant antimicrobial action. The polar surface zone of the compound is 34.14 Å^2. In various models and laws, this has shown a valuable descriptor to quickly gage some ADME properties, especially with regard to memory retention and mind strengthening [35]. Quinone is assimilated through the gastrointestinal (GI) tract and SC tissues. It is mostly discharged unaltered; however mass is killed in conjugation with

Table 8

Optimized geometrical parameters of TCBQ

Sl.No	Geometrical parameters	HF/6-311++	B3LYP/6-311++	Exp. (Ref. [34])
		Bond length, Å		
1	C1—C2	1.50	1.50	1.463
2	C1—C6	1.50	1.50	1.463
3	C1—O7	1.18	1.21	1.216
4	C2—C3	1.32	1.35	1.366
5	C2—Cl8	1.71	1.72	1.76
6	C3—C4	1.50	1.50	1.463
7	C3—Cl9	1.71	1.72	1.76
8	C4—C5	1.50	1.50	1.463
9	C4—O10	1.18	1.21	1.216
10	C5—C6	1.32	1.35	1.366
11	C5—Cl11	1.71	1.72	1.76
12	C6—Cl12	1.71	1.72	1.76
		Bond angle, deg.		
13	C2—C1—C6	117.3	117.0	117.3
14	C2—C1—O7	121.3	121.5	123.0
15	C6—C1—O7	121.3	121.5	123.0
16	C1—C2—C3	121.3	121.5	122.6
17	C1—C2—Cl8	115.2	115.4	—
18	C3—C2—Cl8	123.5	123.2	—
19	C2—C3—C4	121.3	121.5	122.6
20	C2—C3—Cl9	123.5	123.2	—
21	C4—C3—Cl9	115.2	115.4	—
22	C3—C4—C5	117.3	117.0	117.3
23	C3—C4—O10	121.3	121.5	123.0
24	C5—C4—O10	121.3	121.5	123.0
25	C4—C5—C6	121.3	121.5	122.6
26	C4—C5—Cl11	115.2	115.4	—
27	C6—C5—Cl11	123.5	123.2	—
28	C1—C6—C5	121.3	121.5	122.6
29	C1—C6—Cl12	115.2	115.4	—
30	C5—C6—Cl12	123.5	123.2	—

hexuronic, sulfuric and different acids [36].The GI lot serves numerous significant capacities: stomach related, excretory, endocrine, exocrine, etc. Pharmacokinetics affirms that the title compounds has a high GI ingestion. The blood-brain barrier (BBB) is a dynamic and utilitarian neurovascular unit involved in the slender endothelium, astrocytes, pericytes, and extracellular network [37], which is confirmed in this investigation. The more negative the log K_p (with K_p in cm/s), the less permeable the skin is to the compound [38], however, this compound has log K_p (air pervasion) –5.40 cm/s. A medication implied for parenteral use must be profoundly soluble in water to convey an adequate amount of dynamic fixing in the little volume of such pharmaceutical measurements [39]. With various execution on different sets of substances, numerous computational techniques were applied to estimate log $P_{o/w}$.

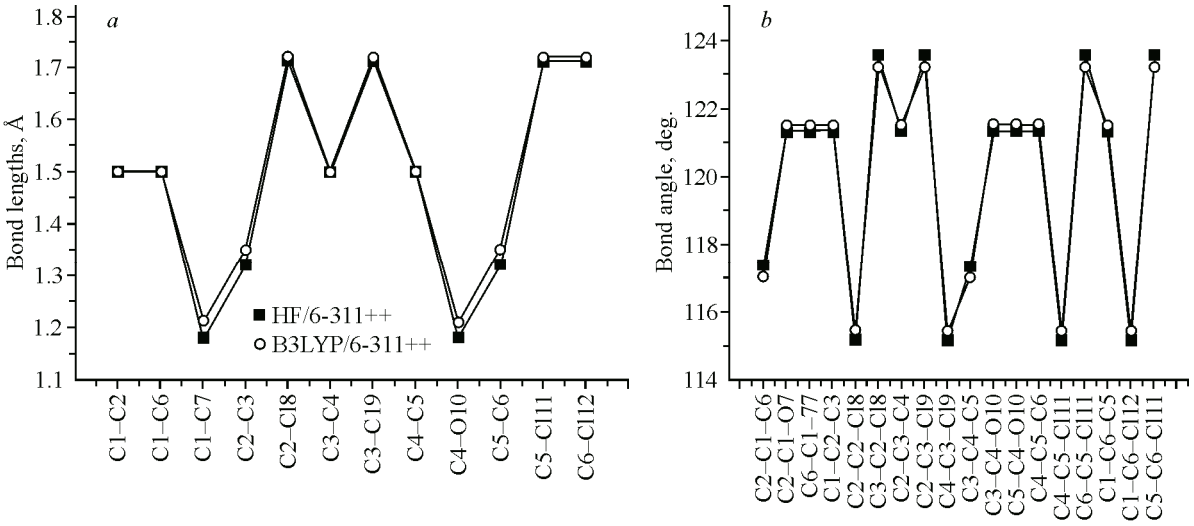

Fig. 8. TCBQ bond lengths (*a*) and bond angles (*b*) calculated by HF and B3LYP

T a b l e 9

Biological activity and ADME *parameters of* TCBQ

Physicochemical Properties	Value	Water Solubility	Value
Form.	$C_6Cl_4O_2$	Log (*S*). (E_{SOL})	–3.49
Mol. weight	245.88 g/mol	Solu.	$7.89e^{-02}$ mg/mL; $3.21e^{-04}$ mol/L
Num. Non-H atoms	12	Cl.	Soluble
Num. Ar. Non-H atoms	0	Log (*S*). (Ali)	–3.78
Fractional C_{sp3}	0.00	Solubility	$4.12e^{-02}$ mg/mL; $1.68e^{-04}$ mol/L
N. rot. bonds	0	Cl.	Soluble
N. H-bond accept.	2	Log *S* (SILICOS-IT)	–3.73
N. H-bond donors	0	Solubility	$4.53e^{-02}$ mg/mL; $1.84e^{-04}$ mol/L
Mol. refrac.	47.48	Class	Soluble
Total PSA	34.14 Å^2		
Lipophilicity Log ($P_{o/w}$)		Drug-likeness	
I LOG P	1.28	Lipinski	Yes; 0 violation
X LOGP3	3.38	Ghose	No; 1 violation: #atoms < 20
W LOGP	2.52	Veb	Yes
M LOGP	1.08	Eg	Yes
SILICOS-IT	3.47	Mue	Yes
Consensus	2.35	Bio.avail Score	55 %
Pharmacokinetics		Medicinal Chemistry	
Gastrointestinal absorption	High	PAINS	2 alerts: ene_one_hal, quinone_A
BBB permeant	Yes	Brenk	1 alert: chinone_1
P-gp substrate	No	Lead like	No; 1 violation: MW < 250
CYP1 $_{A2}$	Yes	Synthetic accessibility	3.08
CYP2 $_{C19}$	No		
CYP2 $_{C9}$	No		
CYP2 $_{D6}$	No		
CYP3 $_{A4}$	No		
Log K_p (Skin per)	–5.40 cm/s		

N o t e. Solu — Solubility; N — Number; Mole — Molar; Refrac — Refractivity; Cl — Class; Form — Formula; Veb — Veber; Eg — Egan; Mue — Muegge; Per — permeation.

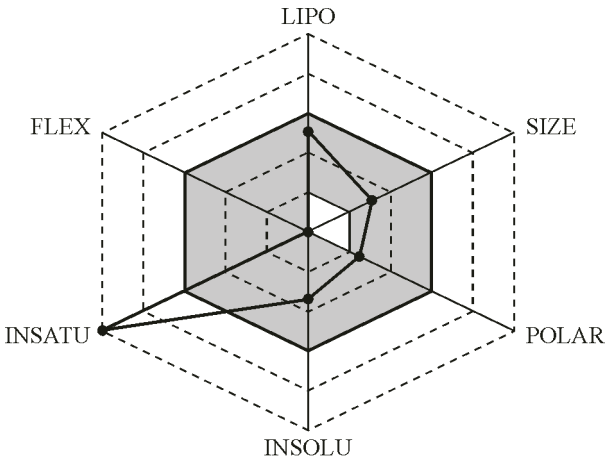

Fig. 9. Bioavailability radar of TCBQ

The bioavailability radar was additionally attracted (Fig. 9) to evaluate the medication resemblance of this compound. Six physicochemical properties were considered: lipophilicity, size, extremity, solvency, adaptability, and immersion. The bioavailability of the compound is 55 %. In Table 9, an enormous assortment of in silico strategies [40] share the purpose of foreseeing ADME boundaries from the subatomic structure. Lipinski et al.′s groundbreaking work examined orally complex mixtures to classify physicochemical searches for a high probability of becoming an oral drug (such as resemblance to medicine) [41]. This is also called the Rule of Five, which portrays the relation between the pharmacokinetic and physicochemical boundaries. The Lipinski standard of five depends on about 91 % of the ADME property. The standard is applied uniquely to the penetration by uninvolved dispersion of medications through cell films; tranquilizers that are effectively moved through cell layers by carrier proteins are special cases to this standard.

CONCLUSIONS

In the current work, endeavors were made from the FTIR, FT-Raman, and FT-NMR spectra as well as the calculated values of HF, B3LYP strategies with 6-311++G(*d*,*p*) for valid recurrence tasks for the TCBQ compound. The TED engagement as a blended mode with different vibrations was around 75 %. In the NBO examination, among all the holding and hostile to holding orbitals, the largest *E*2 values were for C2—C3/C5—C6 → C1—O7/C4—O10 in π—π*. In FMO and UV-Vis investigation, the single most extreme absorption band at 346 nm of HOMO–1 to LUMO is 92 %, which is expected to be the π—π* progress. Mulliken nuclear charges show that C1 and C4 are most electronegative among all carbon atoms in the benzene ring due to the carbonyl substitution. In the NMR investigation, the substitutional ring carbon atoms (C1 and C4) have larger chemical shifts than the other carbon atoms, which is due to the carbonyl conjugation. The MEP graph reveals that carbon, oxygen, and nitrogen atoms have negative potentials, and chlorine atoms have a positive potential in the associated position. The estimation of the second order hyperpolarizability in the title compound shows that it is profoundly pertinent in photography and elastic production as a diminishing agent and a cancer prevention agent. The modification in the bond length or recurrence is a failure of the normal hexagonal uniformity of the benzene ring ascribed to changes in control conveyance on the benzene ring carbon atoms due to replacements with carbonyl groups and chlorine atoms. This would make the thorough analysis of the title compound useful for the potential study of their reactions, used in clinical applications and new products. Such well-performing descriptors ready to appraise important ADME activities are of great help in streamlining pharmacokinetics and assessing the compound.

REFERENCES

1. The Chemistry of the Quinonoid Compounds, Vol. 2, Part 2 / Eds. S. Patai, Z. Rappoport. Wiley, **1988**. https://doi.org/10.1002/9780470772126
2. B. Elvers. Ullmann′s Encyclopedia of Industrial Chemistry. Weinheim, New York: VCH, **1989**.
3. J.M. Lü, S.V. Rosokha, I.S. Neretin, J.K. Kochi. *J. Am. Chem. Soc*., **2006**, *128*, 16708–16719. https://doi.org/10.1021/ja066471o
4. D.R. Buckle, S.J. Collier, M.D. McLaws. In: Encyclopedia of Reagents for Organic Synthesis. John Wiley & Sons, **2005**. https://doi.org/10.1002/047084289x.rd114.pub2
5. Hawley′s Condensed Chemical Dictionary / Ed. R.J. Lewis Sr. New York: Van Nostrand Reinhold, **1992**. https://www.abebooks.com/Hawleys-Condensed-Chemical-Dictionary-12th-Lewis/2940615972/bd (accessed August 24, 2020)
6. New Books. *PANS*, **1972**, *18*, 362–368. https://doi.org/10.1080/09670877209411823
7. C. Bianchini, D. Masi, C. Mealli, A. Meli, G. Martini, F. Laschi, P. Zanello. *Inorg. Chem*., **1987**, *26*, 3683–3693. https://doi.org/10.1021/ic00269a014
8. D.J. Gordon, R.F. Fenske. *Inorg. Chem*., **1982**, *21*, 2907–2915. https://doi.org/10.1021/ic00138a001
9. D.E. Wheeler, J.H. Rodriguez, J.K. McCusker. *J. Phys. Chem. A*, **1999**, *103*, 4101–4112. https://doi.org/10.1021/jp990166q
10. T.N. Al-Sabha, M.S. Al-Enizzi, O.A. Al-Taee. *Eur. Chem. Bull*., **2014**, *3*(4) 377–383.
11. N. El-Najjar, H. Gali-Muhtasib, R.A. Ketola, P. Vuorela, A. Urtti, H. Vuorela. *Phytochem. Rev*., **2011**, *10*, 353–370. https://doi.org/10.1007/s11101-011-9209-1
12. H. Chihara, K. Masukane. *J. Chem. Phys*., **1973**, *59*, 5397–5403. https://doi.org/10.1063/1.1679888
13. M.J. Frisch, G.W. Trucks, H.B. Schlegel, G.E. Scuseria, M.A. Robb, J.R. Cheeseman, G. Scalmani, V. Barone, G.A. Petersson, H. Nakatsuji, X. Li, M. Caricato, A. Marenich, J. Bloino, B.G. Janesko, R. Gomperts, B. Mennucci, H.P. Hratchian, J.V. Ortiz, A.F. Izmaylov, J.L. Sonnenberg, D. Williams-Young, F. Ding, F. Lipparini, F. Egidi, J. Goings, B. Peng, A. Petrone, T. Henderson, D. Ranasinghe, V.G. Zakrzewski, J. Gao, N. Rega, G. Zheng, W. Liang, M. Hada, M. Ehara, K. Toyota, R. Fukuda, J. Hasegawa, M. Ishida, T. Nakajima, Y. Honda, O. Kitao, H. Nakai, T. Vreven, K. Throssell, J.A. Montgomery Jr., J.E. Peralta, F. Ogliaro, M. Bearpark, J.J. Heyd, E. Brothers, K.N. Kudin, V.N. Staroverov, T. Keith, R. Kobayashi, J. Normand, K. Raghavachari, A. Rendell, J.C. Burant, S.S. Iyengar, J. Tomasi, M. Cossi, J.M. Millam, M. Klene, C. Adamo, R. Cammi, J.W. Ochterski, R.L. Martin, K. Morokuma, O. Farkas, J.B. Foresman, D.J. Fox. Gaussian09, Revision A.02. Wallingford, CT: Gaussian, **2016**.
14. R. Dennington, T.A. Keith, J.M. Millam. GaussView, Version 5. Shawnee Mission, KS: Semichem, **2009**.
15. VEDA. Warsaw, Poland: Spectroscopy Molecular Modeling Group, Institute of Nuclear Chemistry and Technology. https://smmg.pl/software/veda (accessed August 25, 2020).
16. F. Weinhold, E.D. Glendening. NBO 6.0 Program Manual: Natural Bond Orbital Analysis Programs. Board of Regents of the University of Wisconsin System on behalf of the Theoretical Chemistry Institute, **1996—2013**. https://docplayer.net/32678675-Nbo-6-0-program-manual-natural-bond-orbital-analysis-programs.html (accessed August 25, 2020).
17. MarvinSketch 5.11.4. ChemAxon, **2012**. https://chemaxon.com (accessed August 25, 2020).
18. A. Daina, O. Michielin, V. Zoete. *Sci. Rep*., **2017**, *7*, 1–13. https://doi.org/10.1038/srep42717
19. G. Varsaİnyi. Assignments for Vibrational Spectra of Seven Hundred Benzene Derivatives. New York: Wiley, **1974**.
20. M. Chao, E. Schempp. *Acta Crystallogr*., *Sect. B: Struct. Crystallogr. Cryst. Chem*., **1977**, *33*, 1557–1564. https://doi.org/10.1107/s0567740877006487
21. S. Gunasekaran, R. Thilak Kumar, S. Ponnusamy. *Spectrochim. Acta*, *Part A*, **2006**, *65*, 1041–1052. https://doi.org/10.1016/j.saa.2006.01.037
22. K. Sarojini, H. Krishnan, C.C. Kanakam, S. Muthu. *Spectrochim. Acta*, *Part A*, **2013**, *108*, 159–170. https://doi.org/10.1016/j.saa.2013.01.060
23. E.A. Velcheva, L.I. Daskalova, I.G. Binev. *Bulg. Chem. Commun*., **2004**, *36*, 230–235.
24. A. Suvitha, S. Periandy, M. Govindarajan, P. Gayathri. *Spectrochim. Acta*, *Part A*, **2015**, *138*. https://doi.org/10.1016/j.saa.2014.10.031
25. M. Govindarajan, M. Karabacak, A. Suvitha, S. Periandy. *Spectrochim. Acta*, *Part A*, **2012**, *89*. https://doi.org/10.1016/j.saa.2011.12.067
26. J. Coates. In: Encyclopedia of Analytical Chemistry / Eds. R.A. Meyers, M.L. McKelvy. Chichester: John Wiley & Sons, **2000**, 10815–10837. https://doi.org/10.1002/9780470027318.a5606
27. P.B. Nagabalasubramanian, S. Periandy, S. Mohan, M. Govindarajan. *Spectrochim. Acta*, *Part A*, **2009**, *73*, 277–280. https://doi.org/10.1016/j.saa.2009.02.044

28. R.L. Frost, A. López, Y. Xi, R. Scholz. *Spectrochim. Acta*, *Part A*, **2014**, *128*, 207–211.https://doi.org/10.1016/j.saa.2014.02.115.
29. N.M. O′Boyle, A.L. Tenderholt, K.M. Langner. *J. Comput. Chem*., **2008**, *29*, 839–845. https://doi.org/10.1002/jcc.20823
30. *p*-Benzoquinone, 2,3,5,6-tetrachloro-. NIST Chemistry WebBook, SRD 69. https://webook.nist.gov/cgi/cbook.cgi?ID=C118752&Mask=400 (accessed August 25, 2020).
31. Chloranil: PubChem Compound Summary for CID 8371. National Center for Biotechnology Information. https://pubchem.ncbi.nlm.nih.gov/compound/Chloranil (accessed August 25, 2020).
32. R. Hollenstein, H.-O. Kalinowski, S. Berger, S. Braun.13C NMR-Spektroskopie. Stuttgart: Georg Thieme, **1984**.
33. P.N. Prasad, D.J. Williams. Introduction to Nonlinear Optical Effects in Molecules and Polymers. New York: John Wiley & Sons, **1991**.
34. A. Rathna, J. Chandrasekhar. *J. Chem. Soc*., *Perkin Trans. 2*, **1991**, 1661–1666. https://doi.org/10.1039/p29910001661.
35. A. Daina, V. Zoete. *ChemMedChem*, **2016**, *11*, 1117–1121. https://doi.org/10.1002/cmdc.201600182
36. G.D. Clayton, F.E. Clayton. Patty′s Industrial Hygiene and Toxicology, Vol. 2A: Toxicology. New York: John Wiley & Sons, **1981**.
37. B.T. Hawkins, T.P. Davis. *Pharmacol. Rev*., **2005**, *57*, 173–185. https://doi.org/10.1124/pr.57.2.4
38. R.O. Potts, R.H. Guy. *Pharm. Res*., **1992**, *9*, 663–669. https://doi.org/10.1023/A:1015810312465
39. K.T. Savjani, A.K. Gajjar, J.K. Savjani. *Int. Scholarly Res. Not*., **2012**, 2012, 195727. https://doi.org/10.5402/2012/195727
40. S. Tian, J. Wang, Y. Li, D. Li, L. Xu, T. Hou. *Adv. Drug Deliv. Rev*., **2015**, *86*, 2–10. https://doi.org/10.1016/j.addr.2015.01.009
41. C.A. Lipinski, F. Lombardo, B.W. Dominy, P.J. Feeney. *Adv. Drug Deliv. Rev*., **2001**, *46*, 3–26. https://doi.org/10.1016/S0169-409X(00)00129-0